PAPER

Check for updates

Wrapping nonspherical vesicles at bio-membranes†

Ajit Kumar Sahu, Rajkumar Malik [ID] and Jiarul Midya [ID] *

The wrapping of particles and vesicles by lipid bilayer membranes is a fundamental process in cellular transport and targeted drug delivery. Here, we investigate the wrapping behavior of nonspherical vesicles, such as ellipsoidal, prolate, oblate, and stomatocytes, by systematically varying the bending rigidity of the vesicle membrane and the tension of the initially planar membrane. Using the Helfrich Hamiltonian, triangulated membrane models, and energy minimization techniques, we predict multiple stable-wrapped states and identify the conditions for their coexistence. Our results demonstrate that softer vesicles bind more easily to initially planar membranes; however, complete wrapping requires significantly higher adhesion strength than rigid vesicles. As membrane tension increases, deep-wrapped states disappear at a triple point where shallow-wrapped, deep-wrapped, and complete-wrapped states coexist. The coordinates of the triple point are highly sensitive to the vesicle shape and stiffness. For stomatocytes, increasing stiffness shifts the triple point to higher adhesion strengths and membrane tensions, while for oblates, it shifts to lower values, influenced by shape changes during wrapping. Oblate shapes are preferred in shallow-wrapped states and stomatocytes in deep-wrapped states. In contrast to hard particles, where optimal adhesion strength for complete wrapping occurs at tensionless membranes, complete wrapping of soft vesicles requires finite membrane tension for optimal adhesion strength. These findings provide insights into the interplay between vesicle deformability, shape, and membrane properties, advancing our understanding of endocytosis and the design of advanced biomimetic delivery systems.

1 Introduction

Cellular transport of information and materials, a fundamental process that ensures the survival and functionality of cells, is typically facilitated by the exchange of particles across lipid membranes.[1,2] The translocation across lipid-bilayer membranes depends on the size, elasticity, shape, and surface functionalization of the particles.[3] Particles smaller than the thickness of the membrane can translocate, causing minimal membrane deformation,[4,5] while particles larger than a few nanometers translocate through endocytosis.[6] Passive endocytosis is a multi-step process that begins with the attachment of the particle to the membrane, followed by wrapping and finally detachment from the membrane.[7] The particle wrapping process, a key aspect of endocytosis, is ubiquitous for both living and nonliving particles, such as drug-carrying nanoparticles,[8] viruses,[9] and parasite invasion into host cells.[10] Membrane tension, regulated by cells through remodeling, plays a critical role in endocytosis: high

tension slows the internalization process, while low tension facilitates membrane invagination and efficient particle uptake.[11–13] Understanding the particle wrapping process can help us optimizing biomedical applications, such as targeted drug delivery using engineered nanoparticles.[14–16]

The wrapping of hard spherical particles at lipid membranes has been extensively investigated in experimental and theoretical studies.[17–21] In general, for the wrapping of hard particles, the size and shape of the particle, the bending rigidity and tension of the membrane, and the adhesion strength of the particle–membrane have been shown to primarily control the process.[22–29] In addition, the initial orientation of the anisotropic hard nanoparticles relative to the adhering membranes influences their wrapping behavior. For example, the wrapping of ellipsoidal[23,30] and spherocylindrical[31] nanoparticles starts with an orientation in which the major axis of the particle is parallel to the membrane surface. After half-wrapping, the orientation of the particle changes, and the major axis becomes perpendicular to the membrane surface. Unlike hard particles, soft particles can deform depending on external constraints;[32,33] the deformability plays an important role in the wrapping process, in addition to the factors that apply to hard particles.

Department of Physics, School of Basic Sciences, Indian Institute of Technology Bhubaneswar, Jatni, Odisha-752050, India. E-mail: jmidya@iitbbs.ac.in

† Electronic supplementary information (ESI) available. See DOI: https://doi.org/10.1039/d5sm00150a

Many biologically relevant particles have anisotropic or non-spherical shapes.[34,35] For example, malaria parasites are typically egg-shaped,[10] mature virions can be ellipsoidal or brick-shaped,[36,37] and vesicular stomatitis viruses (VSV) have bullet shapes.[38] Simulations and experiments show that for ellipsoidal particles the stability of the partial-wrapped over non-wrapped and complete-wrapped states decreases when the bending rigidity of the membrane increases.[39] Living particles also often have the ability to change shape and deformability throughout their life cycles. For example, murine leukemia virus (MLV) and human immunodeficiency virus (HIV) adjust their deformability through internal structural changes, significantly affecting their entry into host cells.[40,41] The mature HIV viral particles are less stiff compared to the immature HIV viral particles, which hinders their complete wrapping at the host cells.[41]

A wide range of synthetic deformable particles with various architectures and customizable mechanical properties can be engineered for the targeted delivery of drugs, including star polymers,[42,43] microgels,[44,45] dendrimers,[46,47] polymer-grafted nanoparticles,[48,49] and vesicles.[8,27,50] The deformability of these particles can be tuned through control parameters that change their molecular architecture or building blocks. For example, the deformability of microgels can be adjusted by changing the cross-link density and electric charge,[51,52] of polymer-grafted nanoparticles by altering the density and length of grafted polymers,[48] and of unilamellar fluid vesicles by modifying the bending rigidity and the osmotic pressure difference.[53] A particularly versatile and well-characterized class of deformable particles is unilamellar vesicles.[27] Free vesicles with fixed membrane areas, variable volumes, and symmetric lipid bilayer membranes assume a spherical shape and may change volumes significantly during wrapping. Nonspherical vesicles with volumes smaller than the maximal volume that can be enclosed by the vesicle membrane and potentially even asymmetric monolayer composition can have a complete zoo of shapes.[54]

In this work, we investigate the wrapping of single non-spherical vesicles with initial ellipsoidal, prolate, oblate, and stomatocytic shapes at initially planar membranes by systematically varying the relative stiffness of the vesicle membranes and the tension of the planar membranes. Using triangulated membranes and energy minimization techniques, we predict energetically stable wrapping states. The systematic increase in adhesion strength leads to transitions of the vesicles from non-wrapped to complete-wrapped states through intermediate shallow-wrapped and deep-wrapped states. Softer vesicles undergo both shape and orientation changes during wrapping, whereas stiffer vesicles exhibit only orientation changes. We calculate wrapping diagrams showing the energetically stable states for various membrane bending rigidities and tensions. As membrane tension increases, the deep-wrapped state becomes destabilized and eventually vanishes at a triple point, where shallow-, deep-, and complete-wrapped states coexist. Beyond the triple point, vesicles exhibit a discontinuous transition from the shallow-wrapped state to the complete-wrapped state. For initial stomatocytes, the triple point shifts to higher membrane tensions and adhesion strengths as the stiffness of

the vesicles increases, while the trend is the opposite for initially oblate ones. In addition, we show that the optimal adhesion strength for the complete wrapping of soft oblate, prolate, and ellipsoidal vesicles occurs at a non-zero membrane tension, unlike rigid particles, which require zero membrane tension. This behavior is related to the shape change of the vesicles during wrapping. Our findings indicate that the initially stomatocyte, oblate and prolate vesicles preferred to be oblate in the shallow-wrapped states and stomatocyte in the deep-wrapped states.

The rest of the manuscript is organized as follows. In Section 2, we introduce the model and the numerical calculation techniques. In Sections 3.1 and 3.2, we show the deformation energy landscapes along with the typical vesicle shapes and characterize the vesicle shapes at various wrapping stages. In Section 3.3, we study the effect of vesicle deformability and in Section 3.4 of membrane tension on the stability of the wrapping states. Finally, in Section 4, we summarize and conclude our study.

2 Model and methods

To study particle wrapping in passive endocytosis, we employ a continuum membrane model, which is applicable to systems where the particle size is at least a few times larger than the thickness of the lipid bilayer membrane.[55,56] In a continuum membrane model, the total energy of the system is calculated using the Helfrich Hamiltonian,[57,58]

$$E = \int_{A_p} dS \left[2\kappa_p H^2 + \sigma \right] + 2\kappa_v \int_{A_v} dS H^2 - w \int_{A_{ad}} dS + \sigma_v A_v + p_v V_v.$$

(1)

Here, $H = (c_1 + c_2)/2$ is the mean curvature, c_1 and c_2 the principal curvatures, A_v the total area of the vesicle, and A_p the area of the initially planar membrane. The adhered area A_{ad} is the area over which the vesicle and the initially planar membrane are attached to each other with adhesion strength w, see Fig. 1(a). The bending rigidities of the vesicle and planar membranes are κ_v and κ_p, respectively, and the tension of the initially planar membrane is σ. The membrane area A_v and the volume V_v of the vesicle are conserved using the Lagrange multipliers σ_v and p_v, respectively. The tension energy of the vesicle is omitted because its membrane area remains constant throughout the wrapping process.

The nonspherical shapes of the vesicles are characterized by reduced volume $v = V_v/V_s$, see Fig. 1(b), and Fig. S1 in the ESI.† Here, V_v is the actual volume of the vesicle with area A_v, and V_s is the volume of a spherical vesicle with the same membrane area. The maximal value, $v = 1$, corresponds to a spherical vesicle. The values of Lagrange multipliers σ_v and p_v depend on the vesicle shape; sudden jumps in their values indicate shape transitions; see Fig. S2 in the ESI.† The stable states for free vesicles with $0.6515 \leq v < 1$ are prolate, with $0.5915 \leq v \leq 0.6515$ are oblate, and with $v \leq 0.5915$ are stomatocytes. We refer to vesicles with $v = 0.95$ as ellipsoidal vesicles.[59]
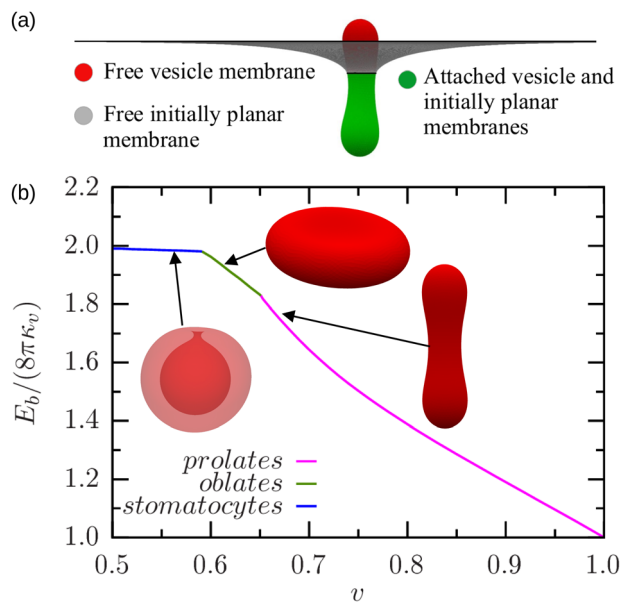
Fig. 1 (a) Schematic representation of a partial-wrapped prolate vesicle at an initially planar membrane. (b) Bending energy of vesicles as a function of reduced volume.

The wrapping fraction $f_w = A_{ad}/A_v$ represents the fraction of the vesicle area that is attached to the initially planar membrane. The value of f_w varies in the range 0 to 1, where $f_w = 0$ corresponds to the non-wrapped (NW) state and $f_w = 1$ to the complete-wrapped (CW) state. The shallow-wrapped (SW) state is defined in the range $0 < f_w \leq 0.5$, and the deep-wrapped (DW) state in the range $0.5 < f_w < 1$. In this work, we are focusing in particular on the wrapping behavior of four vesicle shapes: stomatocyte ($v = 0.55$), oblate ($v = 0.63$), prolate ($v = 0.66$) and ellipsoidal ($v = 0.95$). The selection of vesicle shapes at the phase boundaries between the stomatocyte, oblate, and prolate can result in complex wrapping behaviors compared to prolate vesicles with reduced volumes $v > 0.7$, as previously reported in the literature.[32]

All integrals in eqn (1) are discretized using triangulated surfaces composed of vertices, edges, and facets.[60,61] We initialize the energy and shape calculations with a few large triangles and then iteratively minimize the energy and refine the triangulation until the desired accuracy in energy is achieved; see Fig. S3 in the ESI.† The iterative procedure is important to avoid the need for major shape changes of finely discretized membranes, which would require a high number of minimization steps. Small triangles are used where the membrane is highly curved, and large triangles are used where it is almost planar. In addition, the edges are regularly swapped to maintain the fluidity of the membranes,[62] and vertex-averaging steps ensure that neighboring triangles have similar areas. The numerical calculations are performed with the help of the freely available software Surface Evolver.[63]

For each of our simulations, the membrane area A_v and volume V_v of the vesicle are fixed, while the area A_p of the initially planar membrane is determined through energy minimization, which is appropriate for an ensemble with constant

membrane tension. The simulations are performed by setting $w = 0$ and using f_w as a constraint via a Lagrange multiplier $\tilde{\Gamma}_w$. The total energy of the system can be expressed in terms of reduced units as

$$\tilde{E} = \frac{E}{\pi \kappa_p} = \frac{2}{\pi A_v}\left[\int_{A_p} dS\left[A_v H^2 + \pi \tilde{\sigma}\right] + \kappa_r A_v \int_{A_v} dS H^2\right] \\ + \tilde{\Gamma}_w f_w + \tilde{\sigma}_v A_v + \tilde{p}_v V_v \quad (2)$$

where $\tilde{\sigma} = \sigma A_v/(2\pi\kappa_p)$ is the reduced membrane tension. The bending rigidity ratio $\kappa_r = \kappa_v/\kappa_p$ characterizes the relative deformability of the vesicle with respect to the initially planar membrane.

We perform simulations for different values of f_w in the range $0 < f_w < 1$. For each value of f_w, we initialized the energy minimization with different initial configurations. During this process, the vesicle can adjust its orientation and shape, while the outer patch of the initially planar membrane is constrained to remain in a plane. We calculate the reduced deformation energy as

$$\Delta\tilde{E}'[f_w] = \tilde{E}(f_w) - \tilde{E}(f_w = 0) \\ = \Delta\tilde{E}_{b,v} + \Delta\tilde{E}_{b,p} + \Delta\tilde{E}_{s,p} \quad (3)$$

Here, $\Delta\tilde{E}_{b,v}$, $\Delta\tilde{E}_{b,p}$, and $\Delta\tilde{E}_{s,p}$ represent changes in the bending energy of the vesicle membrane, the bending energy of the initially planar membrane, and the surface energy of the initially planar membrane, respectively. The adhesion energy term is added to eqn (3), resulting in the total deformation energy as

$$\Delta\tilde{E}[f_w] = \Delta\tilde{E}'[f_w] - \tilde{w}f_w, \quad (4)$$

where $\tilde{w} = wA_v/(\pi\kappa_p)$ is the reduced adhesion strength. To identify stable and unstable states, we fit the deformation energy $\Delta\tilde{E}$ at $\tilde{w} = 0$ using a fourth-order polynomial function. Since the energy curve is highly non-monotonic, constructing a single fitting function is challenging. Therefore, we employ a piecewise fitting approach for different ranges of f_w. We apply different adhesion strengths ($\tilde{w}$) to the fitted curves, and find the different global minima in the energy landscape to determine the stable states.[32]

3 Results and discussion

3.1 Wrapping states and deformation energies

Fig. 2 illustrates the wrapping states of nonspherical vesicles at initially planar membranes for various wrapping fractions, f_w. The wrapping process is consistently initiated in regions of the vesicle with the lowest curvature. For a stomatocyte ($v = 0.55$), initial attachment occurs in the "rocket" orientation, where the major axis of the vesicle is perpendicular to the initially planar membrane. As the wrapping progresses, the vesicle deforms to an oblate at $f_w \simeq 0.07$ to minimize the deformation energy, and remains oblate within the range $0.07 \leq f_w \leq 0.5$. For $f_w > 0.5$, the vesicle reverts to its initial stomatocytic shape, persisting in this configuration until the wrapping of the outer sphere of the
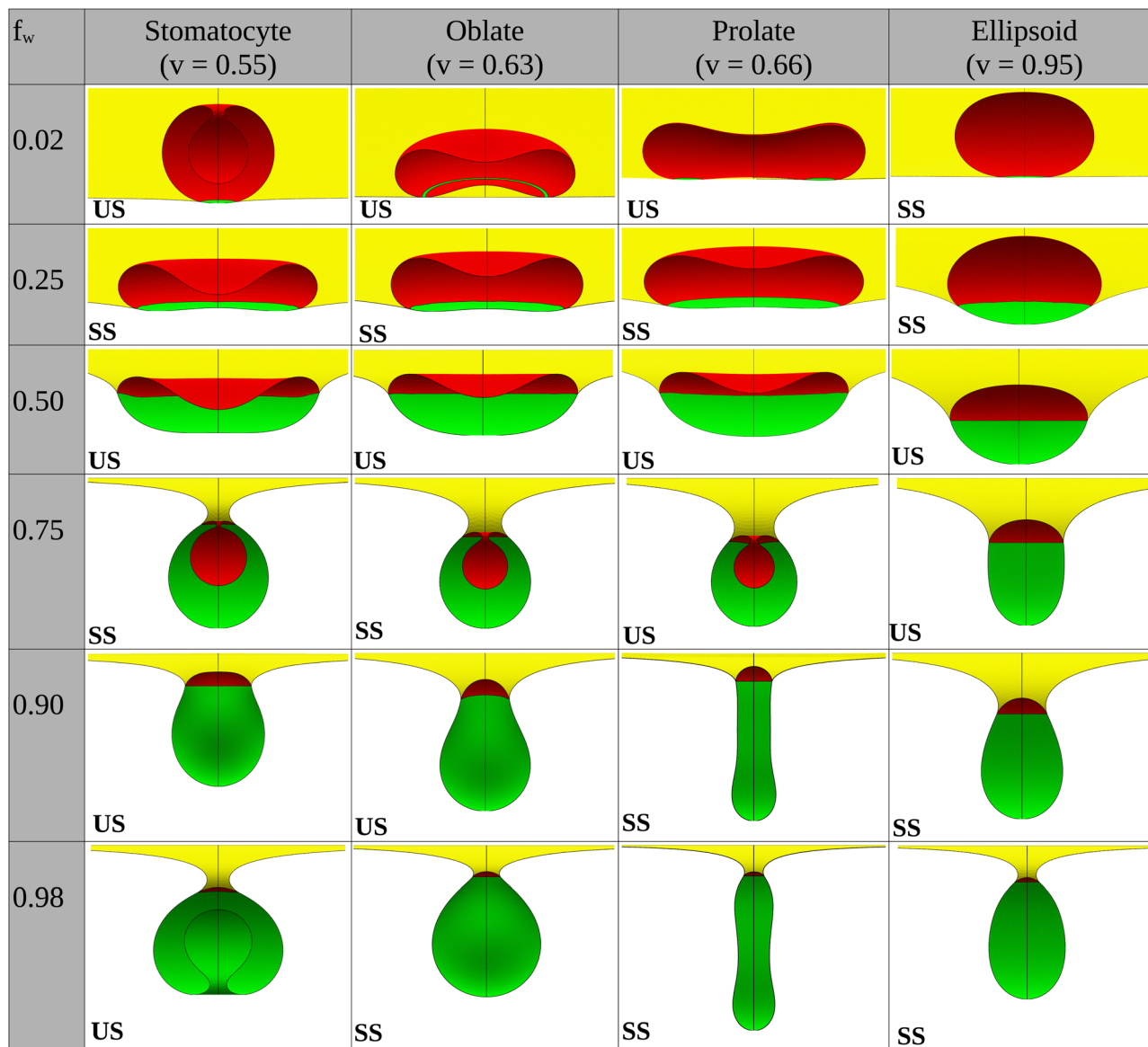
US - Unstable State, SS - Stable State

Fig. 2 Cross-sectional views of partial-wrapped nonspherical vesicles at various wrapping fractions f_w for $\kappa_r = 1$ and $\tilde{\sigma} = 0.5$ along with the indication of stable states (SS) and unstable states (US). Red, green, and yellow colors represent the unattached and attached membrane of the vesicle and the free initially planar membrane, respectively.

stomatocyte is completed. At $f_w \gtrsim 0.75$, the vesicle transforms into a vertical oblate, avoiding the high bending energy costs of the initially planar membrane associated with the wrapping of the inner sphere of the stomatocyte. Finally, at $f_w > 0.9$, the vesicle returns to an inverted stomatocyte. Upon complete wrapping, both the vesicle and the initially planar membrane recover their original shapes.

For an initially oblate vesicle ($v = 0.63$), the attachment to the initially planar membrane begins in a ring-shaped patch with two contact lines, as shown in Fig. 2. As the wrapping fraction f_w increases, the radius of the inner contact line decreases and vanishes at $f_w \approx 0.1$, forming a circular patch with a single contact line, and remains oblate in the range of wrapping

fractions $0.1 < f_w \lesssim 0.5$. At higher f_w values, the initially planar membrane comes into contact with the rim of the oblate, resulting in an increased bending energy cost. This energy cost induces a shape change in the vesicle from oblate to stomatocyte, which persists for $0.5 < f_w \lesssim 0.79$. As f_w increases further, the initially planar membrane needs to bend more to wrap the inner sphere of the stomatocyte, leading to a sharp increase in bending energy. To minimize the overall energy cost, the vesicle compromises its shape and reverts to a vertical oblate for $f_w > 0.79$, maintaining this shape until it is completely wrapped. Similar shape and orientation changes are observed for prolate ($v = 0.66$) and ellipsoidal ($v = 0.95$) vesicles, as illustrated in Fig. 2.

The reduced deformation energy $\Delta\tilde{E}$, calculated using eqn (1)–(4), as a function of the wrapping fraction f_w for various reduced volumes of vesicles ($v = 0.55$, 0.63, 0.66 and 0.95) at a fixed relative stiffness $\kappa_r = \kappa_v/\kappa_p = 1$ and membrane tension $\tilde{\sigma} = 0.5$ is shown in Fig. 3(a)–(d). For an initially stomatocyte ($v = 0.55$), $\Delta\tilde{E}$ increases with f_w in the absence of adhesion energy ($\tilde{w} = 0$), as shown in Fig. 3(a). The energy minimum at $f_w = 0$ suggests that the non-wrapped (NW) state is the stable configuration. However, for adhesion strength $\tilde{w} \simeq 5.3$, a local minimum with the same energy appears for the first time at $f_w \simeq 0.21$ (point 'A'). At this adhesion strength, the vesicle undergoes a binding transition from non-wrapped (NW) to a stable shallow-wrapped (SW) state. The stable shallow-wrapped oblate states can be found for $0.21 \lesssim f_w \lesssim 0.32$. At adhesion strength $\tilde{w} \simeq 15.1$, two energy minima at $f_w \simeq 0.32$ (point 'B') and $f_w \simeq 0.74$ (point 'C') have the same height, which correspond to the discontinuous transition from shallow-wrapped to deep-wrapped W_{sd} where oblate and stomatocyte coexist. At even higher adhesion strength, $\tilde{w} \simeq 33.1$, the deep-wrapped stomatocytic state (point 'D') coexists with the complete-wrapped

(CW) state at $f_w = 1$ (point 'E'); the envelopment transition W_{dc} is also discontinuous. More details about the binding transition, the shallow-to-deep wrapped transition, and the envelopment transition are discussed in the ESI.†

For an oblate ($v = 0.63$), the reduced deformation energy $\Delta\tilde{E}$ as a function of the wrapping fraction f_w is illustrated in Fig. 3(b). The first minimum in $\Delta\tilde{E}$ indicates that the binding transition W_{ns} occurs at the adhesion strength $\tilde{w} \simeq 0.8$ and the wrapping fraction $f_w \simeq 0.16$. The states within the range $0 \leq f_w \lesssim 0.17$ with rim patches, having two contact lines, are on the energy barrier, while the oblate states in the range $0.17 \lesssim f_w \lesssim 0.34$ with single contact line patches are stable. The shallow-to-deep-wrapped transition W_{sd} occurs at adhesion strength $\tilde{w} \simeq 17.5$, where the oblate vesicle at $f_w \simeq 0.34$ (point 'B') coexists with a stomatocyte at $f_w \simeq 0.78$ (point 'C'). Within the deep-wrapped (DW) regime, a deep-wrapped (D_1) to deep-wrapped (D_2) transition W_{dd} is observed for $\tilde{w} \simeq 28.9$, where stomatocytes at $f_w \simeq 0.8$ (point 'D1') coexist with vertical oblates at $f_w \simeq 0.96$ (point 'D2'). Finally, a continuous envelopment transition W_{dc} occurs with an adhesion strength of $\tilde{w} \simeq 55.1$.
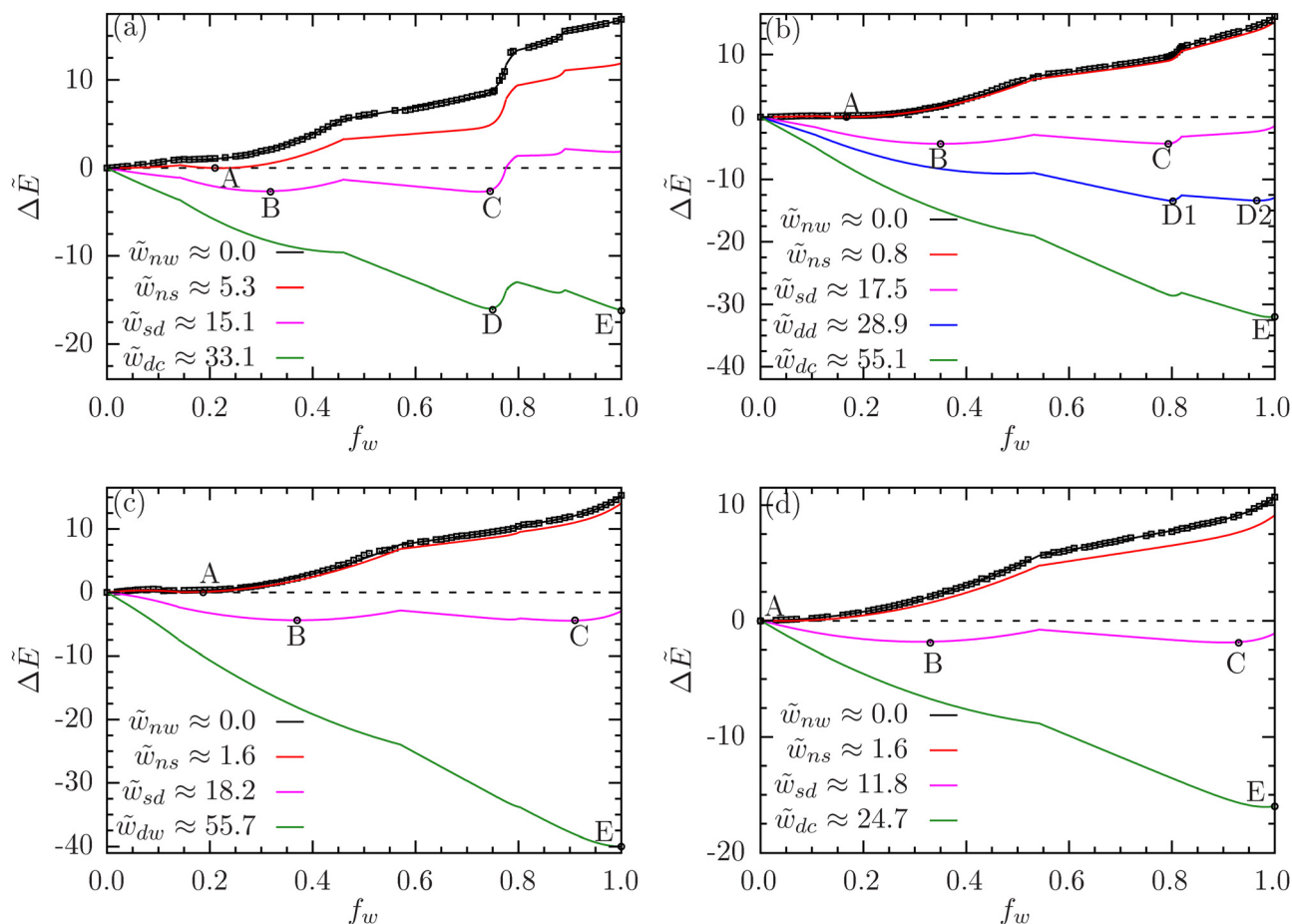

Fig. 3 Deformation energy landscapes of nonspherical vesicles at initially planar membrane as a function of wrapping fraction f_w for vesicles with reduced volumes (a) $v = 0.55$ (stomatocyte), (b) $v = 0.63$ (oblate), (c) $v = 0.66$ (prolate), and (d) $v = 0.95$ (ellipsoid), at bending rigidity ratio $\kappa_r = 1$ and reduced membrane tension $\tilde{\sigma} = 0.5$. The minimal energy states are labeled alphabetically, with A being the wrapping fraction of the shallow-wrapped state for the binding transition, B the wrapping fraction of the shallow-wrapped state, and C the wrapping fraction of the deep-wrapped state for the transition from shallow- to deep-wrapped; D indicates the wrapping fraction of the deep-wrapped state for the envelopment transition; D1 and D2 are wrapping fractions for the deep-wrapped to deep-wrapped transition, and E indicates the complete-wrapped state.

For initially prolate ($v = 0.66$) and ellipsoidal ($v = 0.95$) vesicles, the deformation energy $\Delta \tilde{E}$ as a function of f_w at fixed $\kappa_r = 1$ and $\tilde{\sigma} = 0.5$ is shown in Fig. 3(c) and (d), respectively. The binding transition for initially prolate vesicles ($v = 0.66$) is discontinuous due to the energy barrier associated with the shape transition from prolate to oblate. In contrast, the initially ellipsoidal vesicles ($v = 0.95$) exhibit a continuous binding transition as there is no energy barrier between non-wrapped and shallow-wrapped states; the initial attachment of vesicle occurs in submarine orientation where the major axis is parallel to the initially planar membrane. For both vesicles, the shallow-to-deep wrapped transition is discontinuous due to an energy barrier that arises from changes in shape and orientation of the vesicles; see Fig. 2. However, the envelopment transition is continuous for both the initially prolate ($v = 0.66$) and the initially ellipsoidal ($v = 0.95$) vesicles, as no energy barrier exists between the deep-wrapped and completely wrapped states. Although we focus here on stable states, depending on the values of κ_r, $\tilde{\sigma}$, and $\tilde{w}$ metastable states may also appear along with the stable states.[64] However, determining the vesicle shapes corresponding to these metastable states is challenging without a comprehensive understanding of the entire energy landscape.

3.2 Vesicle shapes during wrapping

The shape of a particle can be quantified using the asphericity,[65,66] calculated from the principal moments (λ_x, λ_y, λ_z) of the gyration tensor. We define the asphericity s^2 as[65]

$$s^2 = \frac{3}{2} \frac{\lambda_x{}^4 + \lambda_y{}^4 + \lambda_z{}^4}{\left(\lambda_x{}^2 + \lambda_y{}^2 + \lambda_z{}^2\right)^2} - \frac{1}{2} \quad (5)$$

For a perfectly spherical particle, the principal moments are equal, $\lambda_x = \lambda_y = \lambda_z$, resulting in asphericity $s^2 = 0$. In contrast, the maximal asphericity $s^2 = 1$ is reached for rod-shaped particles, where $\lambda_x = \lambda_y = 0$ and $\lambda_z \neq 0$ when aligned along the z-axis. During wrapping, the soft vesicles exhibit various shapes depending on the reduced vesicle volume v and the membrane tension $\tilde{\sigma}$. Thus, for nonspherical vesicles, s^2 (> 0) increases with increasing vesicle elongation.

Fig. 4(a) illustrates the asphericity s^2 of the vesicles with various reduced volumes v as a function of the wrapping fraction f_w for $\kappa_r = 1$ and $\tilde{\sigma} = 0.5$. Initially stomatocyte vesicles ($v = 0.55$), resembling two connected spheres, have an asphericity close to zero. In the range $0 < f_w \lesssim 0.07$, the vesicles retain the stomatocytic shape and $s^2 \approx 0$. In stable SW states with $0.07 \lesssim f_w \lesssim 0.5$, the vesicles are oblate with asphericity $s^2 \simeq 0.23$. In the DW state, the vesicles undergo a sequence of shape transitions from stomatocytes to vertical oblates, and then back to inverted stomatocytes. This shape transition leads to a variation in asphericity from $s^2 \approx 0$ in the range $0.5 \lesssim f_w \lesssim 0.75$, to $s^2 \simeq 0.23$ for $0.75 \lesssim f_w \lesssim 0.9$, and finally back to $s^2 \approx 0$ for $f_w \gtrsim 0.9$.

Initially oblate vesicles ($v = 0.63$) retain constant asphericity $s^2 \simeq 0.23$ in the SW state for $0 < f_w \lesssim 0.5$, as they retain their shapes, see Fig. 4(a). However, they transition to deep-wrapped stomatocytes for $0.5 \lesssim f_w \lesssim 0.79$, reducing asphericity to $s^2 \simeq 0$.
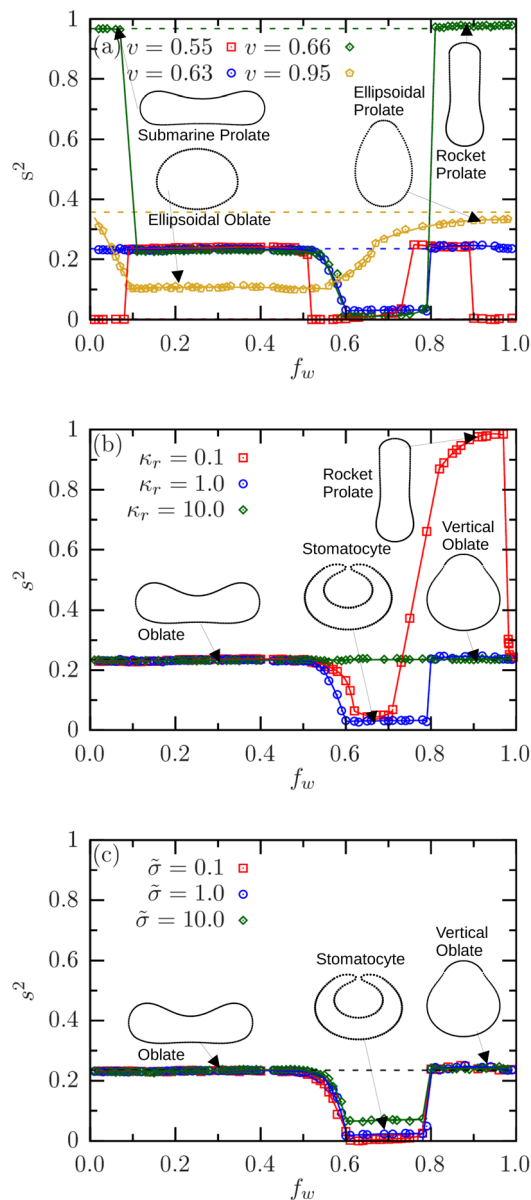

Fig. 4 Asphericity variation with wrapping fraction f_w. (a) Asphericity for vesicles with various v at $\kappa_r = 1$ and $\tilde{\sigma} = 0.5$. (b) Asphericity for various κ_r for $v = 0.63$ at $\tilde{\sigma} = 0.5$. (c) Asphericity for various $\tilde{\sigma}$ for $v = 0.63$ at $\kappa_r = 1$. The dashed lines indicate the asphericities of the corresponding free vesicles.

Within the DW state, the vesicles undergo a transition from stomatocyte to vertical oblate, returning the asphericity to $s^2 \simeq 0.23$ for $0.79 < f_w \leq 1$. In contrast, initially prolate vesicles ($v \simeq 0.66$), which are more elongated, have a high asphericity $s^2 \simeq 0.97$. In SW states, $0.07 \lesssim f_w \lesssim 0.5$, they transition to oblates with $s^2 \simeq 0.23$. In DW states, $0.5 \lesssim f_w \lesssim 0.81$, vesicles adopt stomatocytic states with $s^2 \approx 0$. Finally, for $f_w > 0.81$, the vesicles return to prolates with a rotation of the major axis by $90°$ and asphericities $s^2 \simeq 0.97$. For ellipsoidal vesicles ($v = 0.95$), the asphericity takes a value of $s^2 \simeq 0.1$ when the vesicle adopts an oblate-ellipsoid shape in SW states for $0.1 < f_w \leq 0.5$. In DW states, the vesicles maintain prolate-ellipsoidal shape for $0.5 < f_w \leq 1$ with $s^2 \simeq 0.38$.

Fig. 4(b) illustrates the effects of relative stiffness of the vesicle, κ_r, on the asphericity s^2 for an initially oblate vesicle (v = 0.63) at membrane tension $\tilde{\sigma}$ = 0.5. For soft vesicles ($\kappa_r \lesssim 2.5$), both shape and orientation changes occur during the wrapping process, resulting in variations in asphericity. Across all values of κ_r, the vesicles retain their oblate shape in the SW state for $0 < f_w \lesssim 0.5$, maintaining an asphericity $s^2 \simeq 0.23$. However, in the DW state, the soft vesicles undergo a sequence of shape transitions as the wrapping fraction increases. For example, vesicles with κ_r = 0.1 adopt stomatocytic shapes with $s^2 \approx 0$ for $0.5 \lesssim f_w \lesssim 0.72$, prolate shapes with $s^2 \approx 0.97$ for $0.72 \lesssim f_w \lesssim 0.9$, and vertical oblate shapes with $s^2 \simeq 0.23$ for $f_w \gtrsim 0.95$. In contrast, stiff vesicles (κ_r = 10) undergo only orientation changes, maintaining asphericity $s^2 \simeq 0.23$. Similarly, the effects of membrane tension $\tilde{\sigma}$ on the asphericity of the vesicle are shown in Fig. 4(c) for an oblate (v = 0.63) with relative stiffness κ_r = 1 at various membrane tensions. Across a wide range of wrapping fractions f_w the asphericity s^2 remains nearly constant and is independent of $\tilde{\sigma}$, indicating that the shape of the vesicles is not much affected by changes in membrane tension. It decreases to $s^2 \lesssim 0.1$ for $0.6 \lesssim f_w \lesssim 0.8$, where the vesicle is a stomatocyte. For initially stomatocyte, prolate, and ellipsoidal vesicles, the effects of vesicle stiffness and membrane tension on asphericities are shown in the ESI;† see Fig. S6. The height of the center of mass of the vesicles with respect to the outer patch of the initially planar membrane can similarly indicate both shape change and orientation change during wrapping; see Fig. S7 in the ESI.†

3.3 Effect of vesicle stiffness on the wrapping diagrams

Fig. 5(a)–(d) present the wrapping diagrams for various relative stiffnesses κ_r and reduced adhesion strengths $\tilde{w}$ for vesicles with v = 0.55, 0.63, 0.66, and 0.95 at fixed membrane tension $\tilde{\sigma}$ = 0.5. These wrapping diagrams were extracted from the variation of the deformation energies, $\Delta\tilde{E}$ with f_w; see Fig. S4 in the ESI.† For each value of v, the binding transition W_{ns} shifts to higher adhesion strengths $\tilde{w}$ as κ_r increases, ultimately saturating at a constant value as the deformation of the vesicles is negligible for $\kappa_r \gtrsim 10$. This implies that softer vesicles adhere to the membrane more easily than stiffer ones. In contrast, $\tilde{w}$ for the envelopment transition W_{dc} increases with decreasing κ_r due to the development of a sharp neck at the contact line; see Fig. 2 and 4, indicating that complete wrapping is more challenging for softer vesicles than for stiffer ones. The shape and stiffness
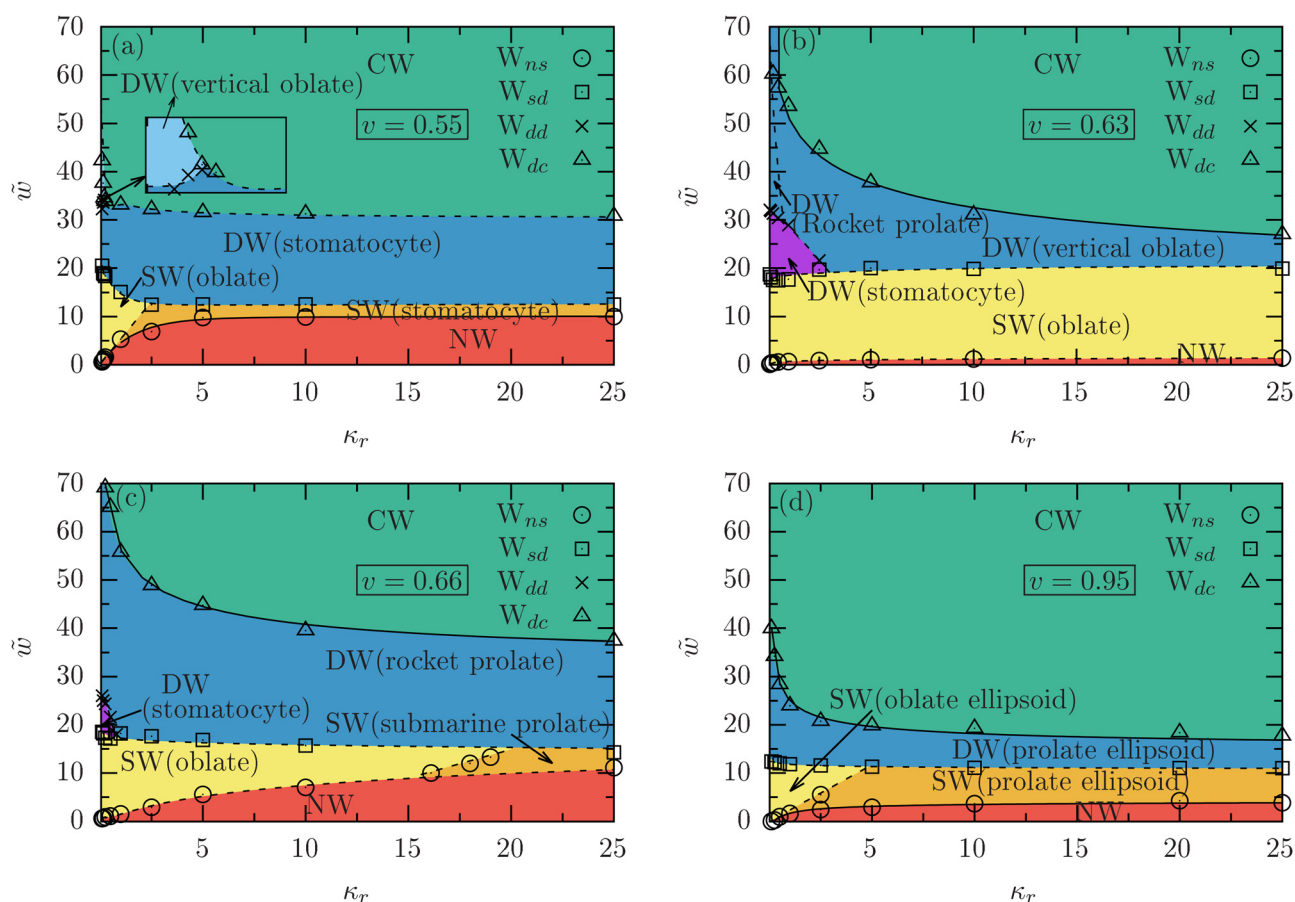

Fig. 5 Wrapping diagrams in the κ_r–$\tilde{w}$ plane at $\tilde{\sigma}$ = 0.5 show stable states: non-wrapped (NW), shallow-wrapped (SW), deep-wrapped (DW), and complete-wrapped (CW) for vesicles with reduced volumes: (a) v = 0.55 (stomatocyte), (b) v = 0.63 (oblate), (c) v = 0.66 (prolate), and (d) v = 0.95 (ellipsoidal). Transitions W_{ns}, W_{sd}, W_{dd}, and W_{dc} indicate NW to SW, SW to DW, DW to DW, and DW to CW transitions, respectively. Solid and dashed lines represent continuous and discontinuous transitions.

of the vesicles also influence the nature of the binding transition, which can be continuous or discontinuous. For example, the binding transition is continuous for ellipsoidal vesicles (v = 0.95) with $\kappa_r \gtrsim 1$ and stiff ($\kappa_r \gtrsim 1$) stomatocyte (v = 0.55) vesicles, while it is discontinuous for soft ($\kappa_r \lesssim 1$) ellipsoidal (v = 0.95), and soft ($\kappa_r \lesssim 2.5$) stomatocyte (v = 0.55) vesicles. For initially oblate (v = 0.63) and prolate (v = 0.66) vesicles, the binding transition is discontinuous for the entire range of κ_r. The envelopment transition is discontinuous for initially stomatocytes and continuous for initially oblates and prolates. The shallow-to-deep-wrapped transition W_{sd} is always discontinuous and shows a moderate increase in $\tilde{w}$ as κ_r decreases.

In the SW state, soft stomatocytes (v = 0.55) with bending rigidity ratio $\kappa_r \lesssim 1$ adopt oblate shapes, while stiff ones with $\kappa_r \gtrsim 2.5$ retain their original shape. For intermediate stiffness, $1 \lesssim \kappa_r \lesssim 2.5$, a discontinuous transition from stomatocyte to oblate occurs as the adhesion strength $\tilde{w}$ increases; see Fig. 5(a). In contrast, oblate (v = 0.63) vesicles consistently maintain a "rocket" orientation for all bending-rigidity ratios; see Fig. 5(b). In the DW state, soft stomatocytes with $\kappa_r < 1$ transition to vertical oblates with increasing $\tilde{w}$. While soft oblate vesicles (v = 0.63) undergo a shape transition as $\tilde{w}$ increases, moving from stomatocyte to rocket prolate for $\kappa_r \lesssim$

0.5 and from stomatocyte to vertical oblate for $0.5 < \kappa_r \lesssim 2.5$. Stiffer vesicles mainly experience an orientation change rather than a shape change. In complete wrapping, regardless of the bending-rigidity ratio, the vesicles return to their initial shapes.

Initially prolate vesicles (v = 0.66) with $\kappa_r \lesssim 16$ transition to oblate in the SW state, while those with $\kappa_r \gtrsim 20$ maintain their shape, see Fig. 5(c). For intermediate stiffness values, $16 \lesssim \kappa_r \lesssim 20$, the vesicles undergo a transition from prolate to oblate with increasing $\tilde{w}$. In the DW state, the vesicles with $\kappa_r < 1$ experience a discontinuous transition from stomatocyte to "rocket" prolate with increasing $\tilde{w}$. In contrast, stiff prolates ($\kappa_r > 1$) show only an orientation change, maintaining the "rocket" prolate state. Similarly, initially ellipsoidal vesicles (v = 0.95) with $1 \lesssim \kappa_r \lesssim 5$ can exhibit a discontinuous transition from prolate to oblate in the SW state as $\tilde{w}$ increases; see Fig. 5(d). Softer shallow-wrapped vesicles ($\kappa_r \lesssim 1$) remain in the oblate state throughout, while stiffer ones ($\kappa_r \gtrsim 5$) remain in the prolate state. In the DW state, all ellipsoidal vesicles adopt the prolate shape with a "rocket" orientation.

Fig. 6 shows the wrapping diagrams in the κ_r–f_w plane for the same parameter values as in Fig. 5. For stomatocytes (v = 0.55) and ellipsoidal (v = 0.95) vesicles with $\kappa_r \gtrsim 1$, initial binding to the initially planar membranes occurs at $f_{w_{ns}} = 0$,
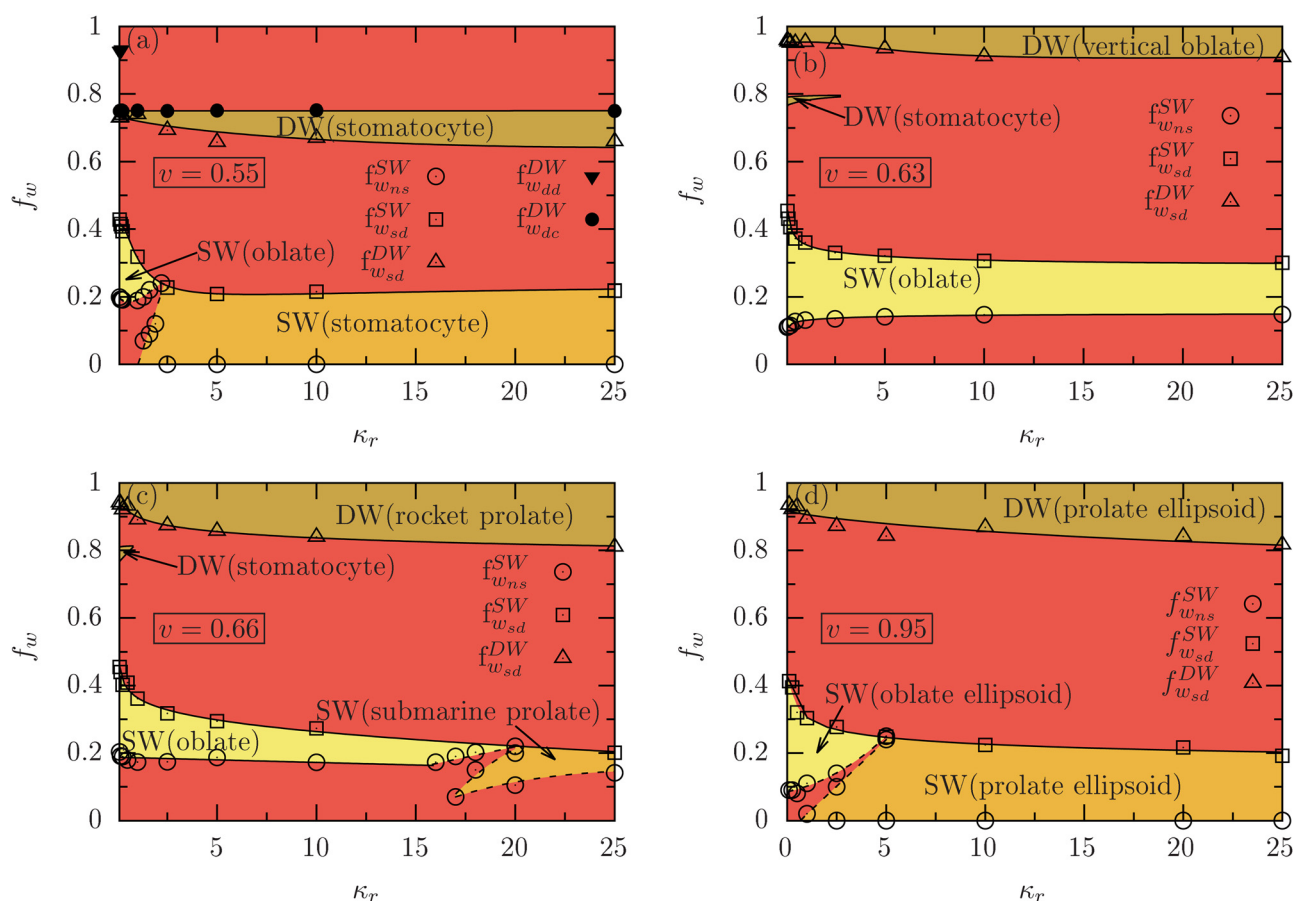

Fig. 6 Wrapping diagrams in the κ_r–f_w at $\bar{\sigma}$ = 0.5 indicating stable non-wrapped (NW), shallow-wrapped (SW), deep-wrapped (DW), and complete-wrapped (CW) states and energy barriers. Data is shown for nonspherical vesicles with reduced volumes (a) v = 0.55 (stomatocyte), (b) v = 0.63 (oblate), (c) v = 0.66 (prolate), (d) v = 0.95 (ellipsoidal). The red-colored regions indicate wrapping fractions f_w for states on the energy barriers.

indicating that the binding transition is continuous. In contrast, soft ($\kappa_r \lesssim 1$) ellipsoidal ($v = 0.95$), soft ($\kappa_r \lesssim 1$) stomatocyte ($v = 0.55$), prolate ($v = 0.66$), and oblate ($v = 0.63$) vesicles show discontinuous binding transitions to $f_{w_{ns}} > 0$. For all reduced volumes, the wrapping fractions $f_{w_{sd}}^{SW}$ and $f_{w_{sd}}^{DW}$ for the coexisting SW to DW states decrease weakly with increasing κ_r and may saturate for higher κ_r. For stomatocyte ($v = 0.55$), the wrapping fractions $f_{w_{dc}}^{DW}$ for the DW states that coexist with the CW state remain constant with increasing κ_r. For initially stomatocytes ($v = 0.55$), the presence of the energy barrier between the DW and CW states indicates that the envelopment transition is discontinuous. In contrast, for oblate ($v = 0.63$), prolate ($v = 0.66$), and ellipsoidal ($v = 0.95$) vesicles, no such energy barrier is found, indicating that the envelopment transition is continuous. The range of accessible wrapping fractions for the DW states increases slightly with increasing v.

In summary, we have studied the wrapping behavior of nonspherical vesicles with different initial shapes—stomatocyte ($v = 0.55$), oblate ($v = 0.63$), prolate ($v = 0.66$), and ellipsoidal ($v = 0.95$)—by systematically varying the relative stiffness (κ_r) of the vesicles at a fixed reduced membrane tension $\tilde{\sigma} = 0.5$. For all the vesicle shapes we have considered, the adhesion strength $\tilde{w}$

for the binding transition decreases with decreasing relative stiffness κ_r, while it increases for envelopment transition. Softer vesicles undergo a sequence of both shape and orientation changes during the wrapping process, while stiffer vesicles exhibit only orientation changes. The binding transition is discontinuous for softer stomatocyte ($v = 0.55$) and ellipsoidal ($v = 0.95$) vesicles, and continuous for the stiffer ones. For initially oblate ($v = 0.63$) and the prolate ($v = 0.66$) vesicles, the binding transition is discontinuous regardless of stiffness. The envelopment transition is continuous for initially oblate ($v = 0.63$), prolate ($v = 0.66$), and ellipsoidal ($v = 0.95$) vesicles, but it is discontinuous for initially stomatocyte ($v = 0.55$) vesicles. For all the considered vesicle shapes, the shallow-to-deep wrapped transition is always discontinuous.

3.4 Effect of membrane tension on the wrapping diagrams

The effects of membrane tension on the wrapping diagrams are shown in Fig. 7 for stomatocyte ($v = 0.55$), oblate ($v = 0.63$), prolate ($v = 0.66$) and ellipsoidal ($v = 0.95$) vesicles, all with fixed relative stiffness $\kappa_r = 1$; the corresponding deformation energies are shown in Fig. S5 in the ESI.† The adhesion strength $\tilde{w}$ for the SW-to-DW transition increases with increasing membrane
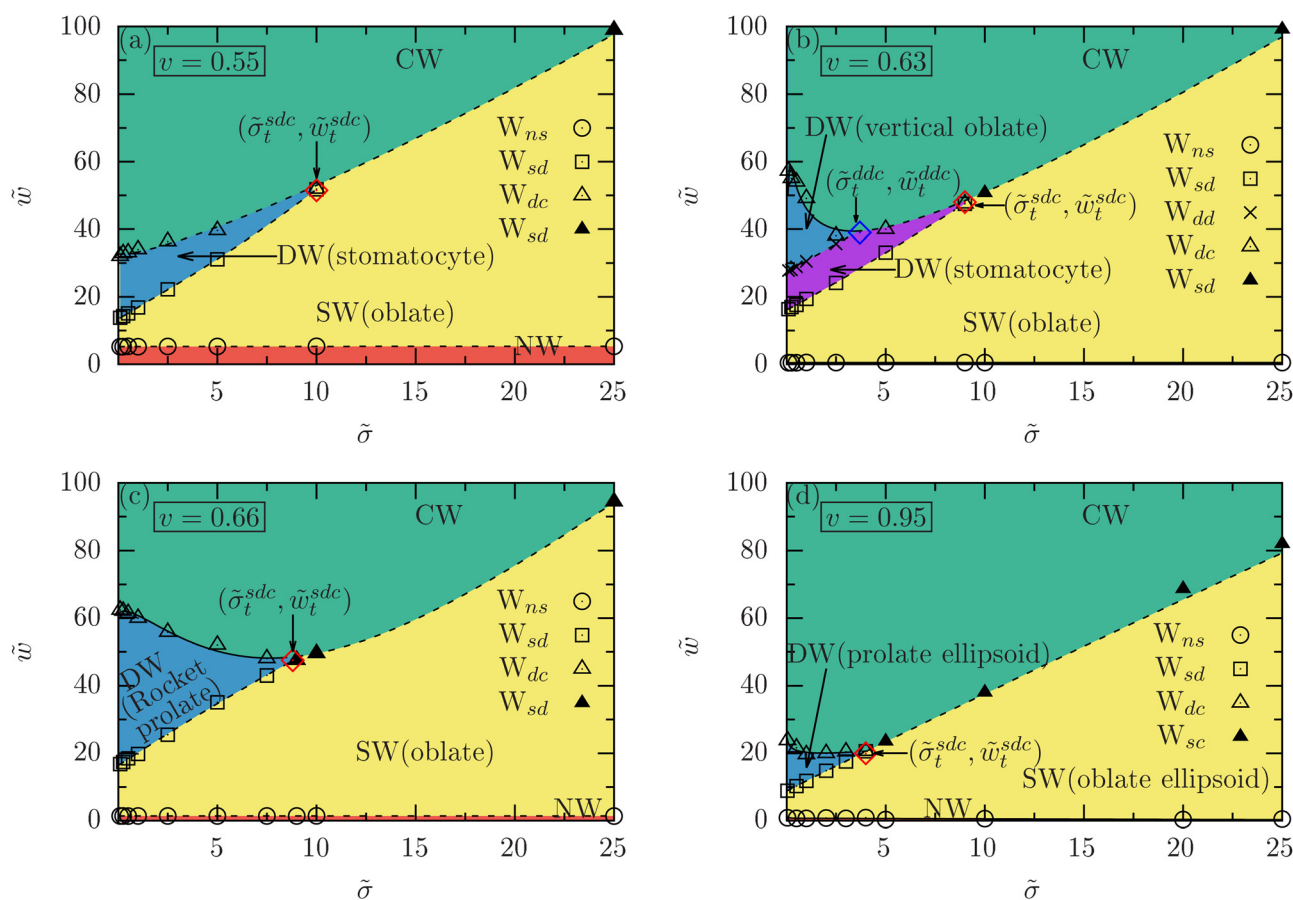

Fig. 7 Wrapping diagrams in the $\tilde{\sigma}-\tilde{w}$ plane at $\kappa_r = 1$. Data is shown for nonspherical vesicles with reduced volumes (a) $v = 0.55$ (stomatocyte), (b) $v = 0.63$ (oblate), (c) $v = 0.66$ (prolate), (d) $v = 0.95$ (ellipsoidal). Stable states and transitions are indicated analogously to Fig. 5; solid lines represent continuous and dashed lines discontinuous transitions, and triple points are highlighted by red diamonds.

tension $\tilde{\sigma}$, due to the increased energy cost in the neck, stabilizing SW over the DW states. As a result, the W_{dc} transition merges with the W_{sd} transition at the triple point $(\tilde{\sigma}_t^{sdc}, \tilde{w}_t^{sdc})$, where the SW, DW, and CW states coexist; the deformation energy landscapes at the triple points are shown in Fig. S8 in the ESI.† Beyond the triple point, the envelopment transition becomes discontinuous, with vesicles undergoing a direct transition from the SW state to the CW state. The adhesion strength $\tilde{w}$ for the binding transition does not change with increasing membrane tension $\tilde{\sigma}$.

For oblates ($v = 0.63$) with a bending-rigidity ratio $\kappa_r = 1$, a deep-wrapped (DW$_1$) to deep-wrapped (DW$_2$) transition occurs at membrane tensions $\tilde{\sigma} \lesssim 4$, where stomatocytes and oblates coexist. For $\tilde{\sigma} \gtrsim 4$, vertical oblate states become unstable, and the DW$_1$-to-DW$_2$ transition vanishes at another triple point $(\tilde{\sigma}_t^{ddc}, \tilde{w}_t^{ddc})$, where two distinct DW states coexist with the CW state; the corresponding deformation energy landscape is shown in Fig. S9 in the ESI.† For initially stomatocytes ($v = 0.55$), the adhesion strength $\tilde{w}$ for complete wrapping gradually increases with increasing membrane tension $\tilde{\sigma}$, since the envelope transition remains discontinuous throughout the membrane tension range $\tilde{\sigma}$. In contrast, for oblates ($v = 0.63$), the envelopment transition is continuous for membrane tensions $0 < \tilde{\sigma} \lesssim \tilde{\sigma}_t^{ddc}$ and discontinuous for $\tilde{\sigma} > \tilde{\sigma}_t^{ddc}$. Similarly, for prolate and ellipsoidal vesicles, the envelopment transition is continuous for membrane tensions $0 < \tilde{\sigma} \lesssim \tilde{\sigma}_t^{sdc}$ and discontinuous for $\tilde{\sigma} \gtrsim \tilde{\sigma}_t^{sdc}$. Consequently, the adhesion strength $\tilde{w}$ for the complete wrapping initially decreases with increasing $\tilde{\sigma}$, reaches its optimal value at the triple point, and beyond the triple point $\tilde{w}$ increases with membrane tension $\tilde{\sigma}$. The wrapping diagram in the f_w–$\tilde{\sigma}$ plane for initially stomatocyte, oblate, prolate, and ellipsoidal vesicles for the same parameter values, as mentioned in Fig. 7, is presented in Fig. S10 in the ESI.†

The coordinates of the triple points in the $\tilde{w}$–$\tilde{\sigma}$ wrapping diagram are influenced by both the bending rigidity ratio κ_r and the reduced volume v of the vesicles. For stomatocytes ($v = 0.55$), the triple point $(\tilde{\sigma}_t^{sdc}, \tilde{w}_t^{sdc})$ shifts to higher values of membrane tension $\tilde{\sigma}$ and adhesion strength $\tilde{w}$ as the bending rigidity ratio κ_r increases; see Fig. 8(a) and Fig. S11 in the ESI.† For high κ_r, the almost spherical shape of the outer surface reduces the cost of wrapping energy for deep-wrapped stomatocytes, and therefore, the regions of stable DW states extend to lower adhesion strengths and higher membrane tensions $\tilde{\sigma}$ with increasing κ_r. However, as the membrane tension $\tilde{\sigma}$ increases, independent of the vesicle shape, the energy cost associated with the neck for the DW states increases, increasing the stability of both the SW and the CW states compared to the DW state.

For an oblate ($v = 0.63$) and $\kappa_r \lesssim 3$, the vesicles transition between an oblate SW and a stomatocyte DW state with increasing adhesion strength, before further transition to oblate DW or CW states, see Fig. 8(a) and Fig. S12 in the ESI.† However, unlike initial stomatocytes, increasing κ_r leads to decreasing tensions $\tilde{\sigma}$ and adhesion strengths $\tilde{w}$ for both triple points $(\tilde{\sigma}_t^{sdd}, \tilde{w}_t^{sdd})$ and $(\tilde{\sigma}_t^{sdc}, \tilde{w}_t^{sdc})$. Increasing the
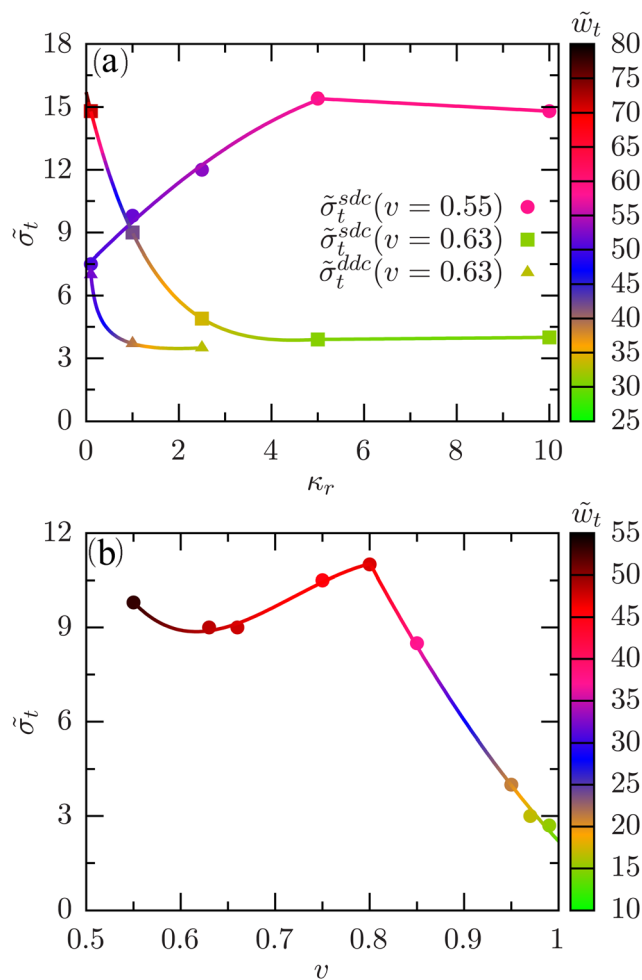

Fig. 8 Membrane tensions $\tilde{\sigma}_t$ and adhesion strengths $\tilde{w}_t$ for the triple points as functions of (a) bending rigidity ratio κ_r for initially stomatocytic ($v = 0.55$, circles) and oblate ($v = 0.63$, squares and triangles) vesicles and (b) for vesicles with various reduced volumes v at $\kappa_r = 1$.

bending-rigidity ratio κ_r stabilizes the oblate states over the stomatocyte states and eventually leads to a direct transition between the oblate SW and the oblate DW or the CW states. The oblate DW state, due to its asymmetrical shape, lacks the advantages that a stomatocytic shape has, and stable states are only found for low tensions.

The triple point $(\sigma_t^{sdc}, \tilde{w}_t^{sdc})$ varies nonmonotonically with reduced volume v at a fixed stiffness of the vesicle $\kappa_r = 1$, as shown in Fig. 8(b). For $0.8 < v < 1$, the triple point moves to higher membrane tensions and adhesion strengths as v decreases. This occurs because the vesicle becomes more elongated with decreasing v, increasing the stability of the deep-wrapped prolate states relative to the shallow-wrapped oblate states. In contrast, for $0.55 < v < 0.8$, the vesicles tend to adopt an oblate shape in the SW state and a stomatocyte shape in the DW state. Consequently, the triple point shifts to lower membrane tensions and adhesion strengths.

In summary, we have investigated the wrapping behavior of nonspherical vesicles with different initial shapes—stomatocyte ($v = 0.55$), oblate ($v = 0.63$), prolate ($v = 0.66$), and ellipsoidal

(v = 0.95)—by systematically varying the reduced tension ($\tilde{\sigma}$) of an initially planar membrane at a fixed bending rigidity ratio κ_{r} = 1. The adhesion strength $\tilde{w}$ for the binding transition remains constant with increasing membrane tension $\tilde{\sigma}$. The stability of the shallow-wrapped state increases with increasing $\tilde{\sigma}$. At high membrane tension $\tilde{\sigma}$, the deep-wrapped state disappears at a triple point where the shallow-wrapped, deep-wrapped, and completely wrapped states coexist. For initially oblate vesicles (v = 0.63), an additional triple point is observed where two distinct deep-wrapped states (DW$_1$ and DW$_2$) coexist with the completely wrapped state. We have shown the coordinates of the triple point is influenced by both the bending rigidity ratio κ_{r} and the reduced volume v of the vesicles. For initially oblate (v = 0.63), prolate (v = 0.66), and ellipsoidal (v = 0.95) vesicles, the triple point marks the minimum adhesion strength $\tilde{w}$ for complete wrapping which occurs at a finite membrane tension.

4 Conclusions and outlook

We calculated the shapes, orientations, and energies for the wrapping of initially prolate, oblate, and stomatocytic vesicles at initially planar membranes. A systematic variation of reduced volumes, bending rigidity ratios, and membrane tensions leads to a rich phase behavior. Whereas shallow-wrapped states are often oblate, deep-wrapped states stabilize stomatocytic shapes. Transitions between shallow-wrapped and deep-wrapped states are always discontinuous, whereas the binding and envelopment transitions can be either continuous or discontinuous depending on vesicle stiffness and membrane tension. Softer vesicles undergo major shape changes during wrapping, while stiffer ones show only orientation changes, and at high tensions, the transition can occur directly from SW to CW states. Stomatocytic shapes can, because of their near-spherical shape, stabilize deep-wrapped over shallow-wrapped states and also for initially oblate and prolate vesicles. For soft vesicles, the binding transition is shifted to lower adhesion strengths, and the envelopment transition to higher adhesion strengths, in agreement with previous studies.[32,33]

Increasing membrane tension destabilizes deep-wrapped states that vanish at a triple point, leading to the coexistence of shallow-, deep-, and complete-wrapped states. Vesicle asphericities and triple-point coordinates can be used to systematically characterize phase diagrams as functions of elastic parameters. With increasing stiffness, the triple points between the shallow-wrapped, deep-wrapped, and complete-wrapped states shift to lower tensions and adhesion strengths for initially oblate vesicles and to higher values for initially stomatocytic vesicles. For oblate, prolate and ellipsoidal vesicles, the optimal membrane tension for uptake is finite, indicating that the adhesion strength required for complete wrapping is not the lowest for vanishing tension, as expected for hard particles.[19,23,25] Because cells can regulate their membrane tension,[67,68] non-spherical vesicles can favor endocytosis or shallow-wrapped states; the latter may eventually facilitate fusion and direct delivery of the vesicle volume to the cytosol.[8]

Vesicles are a versatile class of elastic particles, exhibiting unique behaviors not observed in particles with 3D elasticity, such as polymeric particles. In particular, in the regime of stable deep-wrapped states, vesicles show internal discontinuous shape transitions with stomatocytic states extending to higher membrane tensions. Studying initial vesicle shapes close to the phase boundaries between stomatocytic, oblate, and prolate vesicles leads to an intriguing qualitatively novel finding compared to prolate vesicles with reduced volumes v > 0.7, which we studied earlier.[32] Our findings on the wrapping of nonspherical vesicles at initially planar membranes provide valuable insights for designing tailored deformable particles, with potential applications in membrane attachment, fusion, and endocytosis.

This work highlights how vesicle shape, deformability, and membrane tension influence wrapping transitions on initially planar membranes. While our current model assumes a contact potential, many realistic systems involve long-range adhesive interactions.[69] Thus, future studies could include wrapping nonspherical vesicles at lipid membranes by systematically varying the range of adhesion interaction potential to mimic realistic systems. For vesicles with very low reduced volumes, large energy barriers may lead to metastable shapes,[70] which can make the wrapping transitions more complex. Investigating the wrapping behavior of metastable states of such vesicles could be a valuable extension of this work. Additionally, membrane deformations induce membrane-mediated interactions, which become particularly important in crowded environments. Predicting these interaction potentials between multiple vesicles could offer insights into the aggregation behavior of virions on biomembranes. However, the knowledge we gained from this work may also contribute to biomedical applications, particularly targeted drug delivery using deformable nanoparticles.

Author contributions

Data availability

The data used in this study are available in the main manuscript or the ESI.† Additional raw data and analysis scripts can be obtained from the corresponding author upon request.

Conflicts of interest

There are no conflicts to declare.

Acknowledgements

Notes and references

1 T. Pomorski, S. Hrafnsdóttir, P. F. Devaux and G. van Meer, *Semin. Cell Dev. Biol.*, 2001, **12**, 139–148.

2 H. Sprong, P. Van Der Sluijs and G. Van Meer, *Nat. Rev. Mol. Cell Biol.*, 2001, **2**, 504–513.

3 S. Dasgupta, T. Auth and G. Gompper, *J. Phys.: Condens. Matter*, 2017, **29**, 373003.

4 S. Pogodin, M. Werner, J.-U. Sommer and V. A. Baulin, *ACS Nano*, 2012, **6**, 10555–10561.

5 M. Werner, J. Bathmann, V. A. Baulin and J.-U. Sommer, *ACS Macro Lett.*, 2017, **6**, 247–251.

6 B. S. Joshi, M. A. de Beer, B. N. G. Giepmans and I. S. Zuhorn, *ACS Nano*, 2020, **14**, 4444–4455.

7 A. Hubbard, *Curr. Opin. Cell Biol.*, 1989, **1**, 675–683.

8 S. Kube, N. Hersch, E. Naumovska, T. Gensch, J. Hendriks, A. Franzen, L. Landvogt, J.-P. Siebrasse, U. Kubitscheck and B. Hoffmann, *et al.*, *Langmuir*, 2017, **33**, 1051–1059.

9 T. Wiegand, M. Fratini, F. Frey, K. Yserentant, Y. Liu, E. Weber, K. Galior, J. Ohmes, F. Braun and D.-P. Herten, *et al.*, *Nat. Commun.*, 2020, **11**, 32.

10 S. Dasgupta, T. Auth, N. S. Gov, T. J. Satchwell, E. Hanssen, E. S. Zuccala, D. T. Riglar, A. M. Toye, T. Betz, J. Baum and G. Gompper, *Biophys. J.*, 2014, **107**, 43–54.

11 Q. Yu, S. Dasgupta, T. Auth and G. Gompper, *Nano Lett.*, 2020, **20**, 1662–1668.

12 T. A. Masters, B. Pontes, V. Viasnoff, Y. Li and N. C. Gauthier, *Proc. Natl. Acad. Sci. U. S. A.*, 2013, **110**, 11875–11880.

13 P. Sens and M. S. Turner, *Phys. Rev. E: Stat., Nonlinear, Soft Matter Phys.*, 2006, **73**, 031918.

14 M. J. Mitchell, M. M. Billingsley, R. M. Haley, M. E. Wechsler, N. A. Peppas and R. Langer, *Nat. Rev. Drug Discovery*, 2021, **20**, 101–124.

15 W. H. De Jong and P. J. Borm, *Int. J. Nanomed.*, 2008, **3**, 133–149.

16 C. Barbe, J. Bartlett, L. Kong, K. Finnie, H. Q. Lin, M. Larkin, S. Calleja, A. Bush and G. Calleja, *Adv. Mater.*, 2004, **16**, 1959–1966.

17 C. Van Der Wel, A. Vahid, A. Šarić, T. Idema, D. Heinrich and D. J. Kraft, *Sci. Rep.*, 2016, **6**, 32825.

18 M. Raatz, R. Lipowsky and T. R. Weikl, *Soft Matter*, 2014, **10**, 3570–3577.

19 M. Deserno and T. Bickel, *Europhys. Lett.*, 2003, **62**, 767.

20 R. Lipowsky and H.-G. Döbereiner, *Europhys. Lett.*, 1998, **43**, 219.

21 S. van der Ham, J. Agudo-Canalejo and H. R. Vutukuri, *ACS Nano*, 2024, **18**, 10407–10416.

22 A. Azadbakht, B. Meadowcroft, T. Varkevisser, A. Šarić and D. J. Kraft, *Nano Lett.*, 2023, **23**, 4267–4273.

23 S. Dasgupta, T. Auth and G. Gompper, *Nano Lett.*, 2014, **14**, 687–693.

24 W. Jiang, B. Y. Kim, J. T. Rutka and W. C. Chan, *Nat. Nanotechnol.*, 2008, **3**, 145–150.

25 S. Dasgupta, T. Auth and G. Gompper, *Soft Matter*, 2013, **9**, 5473–5482.

26 A.-S. Smith and U. Seifert, *Phys. Rev. E: Stat., Nonlinear, Soft Matter Phys.*, 2005, **71**, 061902.

27 U. Seifert, *Adv. Phys.*, 1997, **46**, 13–137.

28 A. H. Bahrami, *Soft Matter*, 2013, **9**, 8642–8646.

29 A. Scotti, M. F. Schulte, C. G. Lopez, J. J. Crassous, S. Bochenek and W. Richtering, *Chem. Rev.*, 2022, **122**, 11675–11700.

30 C. Huang, Y. Zhang, H. Yuan, H. Gao and S. Zhang, *Nano Lett.*, 2013, **13**, 4546–4550.

31 A. Sharma, Y. Zhu, E. J. Spangler and M. Laradji, *J. Chem. Phys.*, 2022, **156**, 234901.

32 J. Midya, T. Auth and G. Gompper, *ACS Nano*, 2023, **17**, 1935–1945.

33 X. Yi, X. Shi and H. Gao, *Phys. Rev. Lett.*, 2011, **107**, 098101.

34 Y. Hatano, M. Yoshida, F. Uno, S. Yoshida, N. Osafune, K. Ono, M. Yamada and S. Nii, *J. Electron Microsc.*, 2001, **50**, 113–124.

35 D. K. Cureton, R. H. Massol, S. Saffarian, T. L. Kirchhausen and S. P. J. Whelan, *PLoS Pathog.*, 2009, **5**, e1000394.

36 R. C. Condit, N. Moussatche and P. Traktman, *Adv. Virus Res.*, 2006, **66**, 31–124.

37 J. Liu, S. Corroyer-Dulmont, V. Pražák, I. Khusainov, K. Bahrami, S. Welsch, D. Vasishtan, A. Obarska-Kosińska, S. R. Thorkelsson, K. Grünewald, E. R. J. Quemin, B. Turoňová and J. K. Locker, *Nat. Struct. Mol. Biol.*, 2024, **31**, 1105–1113.

38 P. Ge, J. Tsao, S. Schein, T. J. Green, M. Luo and Z. H. Zhou, *Science*, 2010, **327**, 689–693.

39 X. Liu, T. Auth, N. Hazra, M. F. Ebbesen, J. Brewer, G. Gompper, J. J. Crassous and E. Sparr, *Proc. Natl. Acad. Sci. U. S. A.*, 2023, **120**, e2217534120.

40 H.-B. Pang, L. Hevroni, N. Kol, D. M. Eckert, M. Tsvitov, M. S. Kay and I. Rousso, *Retrovirology*, 2013, **10**, 4.

41 N. Kol, M. Gladnikoff, D. Barlam, R. Z. Shneck, A. Rein and I. Rousso, *Biophys. J.*, 2006, **91**, 767–774.

42 C. Likos, H. Löwen, M. Watzlawek, B. Abbas, O. Jucknischke, J. Allgaier and D. Richter, *Phys. Rev. Lett.*, 1998, **80**, 4450.

43 J. M. Ren, T. G. McKenzie, Q. Fu, E. H. Wong, J. Xu, Z. An, S. Shanmugam, T. P. Davis, C. Boyer and G. G. Qiao, *Chem. Rev.*, 2016, **116**, 6743–6836.

44 M. Brugnoni, A. Scotti, A. A. Rudov, A. P. Gelissen, T. Caumanns, A. Radulescu, T. Eckert, A. Pich, I. I. Potemkin and W. Richtering, *Macromolecules*, 2018, **51**, 2662–2671.

45 F. A. Plamper and W. Richtering, *Acc. Chem. Res.*, 2017, **50**, 131–140.

46 J. Chen, D. Zhu, B. Lian, K. Shi, P. Chen, Y. Li, W. Lin, L. Ding, Q. Long and Y. Wang, *et al.*, *Proc. Natl. Acad. Sci. U. S. A.*, 2023, **120**, e2220787120.

47 U. Boas and P. M. Heegaard, *Chem. Soc. Rev.*, 2004, **33**, 43–63.

48 J. Midya, Y. Cang, S. A. Egorov, K. Matyjaszewski, M. R. Bockstaller, A. Nikoubashman and G. Fytas, *Nano Lett.*, 2019, **19**, 2715–2722.

49 D. Vlassopoulos and G. Fytas, From polymers to colloids: engineering the dynamic properties of hairy particles, in *High Solid Dispersions*, 2010, pp. 1–54.

50 I. Hoffmann, C. Hoffmann, B. Farago, S. Prévost and M. Gradzielski, *J. Chem. Phys.*, 2018, **148**, 104901.

51 T. Höfken, U. Gasser, S. Schneider, A. V. Petrunin and A. Scotti, *Macromol. Rapid Commun.*, 2024, **45**, 2400043.

52 C. Strauch and S. Schneider, *Soft Matter*, 2023, **19**, 938–950.

53 D. Vorselen, F. C. MacKintosh, W. H. Roos and G. J. Wuite, *ACS Nano*, 2017, **11**, 2628–2636.

54 U. Seifert, *Adv. Phys.*, 1997, **46**, 13–137.

55 R. Groza, K. V. Schmidt, P. M. Müller, R. Ronchi, C. Schlack-Leigers, U. Neu, R. Puchkov, D. Dimova, C. Matthaeus, J. Taraska, T. R. Weikl and H. Ewers, *Nat. Commun.*, 2024, **15**, 2767.

56 N. Baruah, J. Midya, G. Gompper, A. K. Dasanna and T. Auth, *Biophys. J.*, 2025, **124**, 740–752.

57 W. Helfrich, *Z. Naturforsch., C*, 1973, **28**, 693–703.

58 H. Deuling and W. Helfrich, *J. Phys.*, 1976, **37**, 1335–1345.

59 W. Góźdź, *Langmuir*, 2007, **23**, 5665–5669.

60 W. Pezeshkian, M. König, T. A. Wassenaar and S. J. Marrink, *Nat. Commun.*, 2020, **11**, 2296.

61 G. Gompper and D. M. Kroll, *Statistical Mechanics of Membranes and Surfaces*, World Scientific, 2004, pp. 359–426.

62 D. Kroll and G. Gompper, *Science*, 1992, **255**, 968–971.

63 K. A. Brakke, *Exp. Math.*, 1992, **1**, 141–165.

64 H. Noguchi, A. Sakashita and M. Imai, *Soft Matter*, 2015, **11**, 193–201.

65 J. Midya, M. Rubinstein, S. K. Kumar and A. Nikoubashman, *ACS Nano*, 2020, **14**, 15505–15516.

66 H. Noguchi and G. Gompper, *Phys. Rev. Lett.*, 2004, **93**, 258102.

67 E. Sitarska and A. Diz-Muñoz, *Curr. Opin. Cell Biol.*, 2020, **66**, 11–18.

68 M. P. Sheetz and J. Dai, *Trends Cell Biol.*, 1996, **6**, 85–89.

69 M. Raatz and T. R. Weikl, *Adv. Mater. Interfaces*, 2017, **4**, 1600325.

70 A. H. Bahrami and G. Hummer, *ACS Nano*, 2017, **11**, 9558–9565.